Interferometric polarization control

David T. Chuss, Edward J. Wollack, S. Harvey Moseley, and Giles Novak

We develop the Jones and Mueller matrices for structures that allow control of the path length difference between two linear orthogonal polarizations and consider the effect of placing multiple devices in series. Specifically, we find that full polarization modulation (measurement of Stokes Q, U, and V) can be achieved by placing two such modulators in series if the relative angles of the beam-splitting grids with respect to the analyzer orientation are appropriately chosen. Such a device has several potential advantages over a spinning wave plate modulator for measuring astronomical polarization in the far infrared through millimeter: (i) The use of small, linear motions eliminates the need for cryogenic rotational bearings; (ii) the phase flexibility allows measurement of circular as well as linear polarization; and (iii) this architecture allows for both multiwavelength and broadband modulation. We also present initial laboratory results.

OCIS codes: 230.5440, 260.5430, 120.5410.

1. Introduction

Astronomical polarimetry is currently drawing much attention, mostly due to the anticipated high-sensitivity searches for the so-called B modes of the cosmic microwave background (CMB) polarization. These signatures of gravitational waves produced during the inflationary epoch are expected to provide a direct measurement of the energy scale of inflation. The amplitude of the B modes is theorized to be 10^{-7} to 10^{-9} of the power of the CMB, and so its measurement will require a good modulation strategy and control over systematic artifacts.

The emission from magnetically aligned dust in our galaxy provides a contaminant that will have to be understood in order to correctly extract the B modes from the total signal. On the other hand, this polarized emission provides a tool for analyzing the role of magnetic fields in star formation, and with the advent of multiwavelength submillimeter and far infrared photometers such as the submillimeter common-use bolometer array (SCUBA2)[1] and the high angular-resolution widefield camera/Stratospheric Observatory for Infrared Astronomy (HAWC/SOFIA),[2] there is an opportunity to expand this field of study. To take advantage of the new detector technology that will be coming online in the next few years, it is necessary to develop the polarization modulation technology that will enable the conversion of these photometers into polarimeters.

Fundamentally, partial polarization arises as a result of statistical correlations between the electric field components in the plane perpendicular to the propagation direction. These correlations are represented by complex quantities, but in the measurement of polarized light, it is often convenient to use real linear combinations of these correlations, namely, the Stokes parameters, I, Q, U, and V.

It is possible to trace the polarization state of radiation through an optical system by determining the transformations that describe the mapping of the input to output polarization states. We are specifically concerned with the class of optical elements for which Stokes I is decoupled from the other Stokes parameters. For this class of elements, the polarization,

$$P^2 = Q^2 + U^2 + V^2, \tag{1}$$

is constant. This equation can be interpreted to describe the points on the surface of a sphere in a 3D space having Q, U, and V as coordinate axes. This sphere is known as the Poincaré sphere, and the action of any given ideal polarization modulator can be represented by a rotation (and/or an inversion) in this space. Such an operation corresponds to the introduction of a phase delay between orthogonal polarizations, which is the physical mechanism at work

D. T. Chuss (David.T.Chuss@nasa.gov), E. J. Wollack, and S. H. Moseley are with the NASA Goddard Space Flight Center, Code 665, Greenbelt, Maryland 20771. G. Novak is with the Department of Physics and Astronomy, Northwestern University, 2145 Sheridan Road, Evanston, Illinois 60208.

Received 11 October 2005; revised 5 January 2006; accepted 25 January 2006; posted 31 January 2006 (Doc. ID 65313).

0003-6935/06/215107-11$15.00/0

in a polarization modulator. The two degrees of freedom of any given transformation are the magnitude of the introduced phase delay and a parameter describing the basis used to define the phase delay. These two parameters directly define the orientation and the magnitude of the rotation on the Poincaré sphere: The rotation axis is defined by the sphere diameter connecting the two polarization states between which the phase is introduced, and the magnitude of the rotation is equal to that of the introduced phase.[3]

In order to measure the polarized part of a partially polarized signal, it is desirable to separate the polarized part of the signal from the unpolarized part. This is especially crucial when the fractional polarization of the signal is small. One way to do this is to methodically change, or modulate, the polarized part of the signal (by changing one of the parameters of the polarization modulator) while leaving the unpolarized part unaffected. Periodic transformations in Poincaré space can accomplish this encoding of the polarized component of the signal for subsequent synchronous demodulation and detection. A convenient way of formulating the problem is to envision a detector that is sensitive to Stokes Q when projected onto the sky in the absence of modulation. The polarization modulator then systematically changes the polarization state to which the detector is sensitive. By measuring the output signal, the polarization state of the light can be completely characterized.

A common implementation of such a polarization modulator is a dielectric birefringent plate.[4] A birefringent plate consists of a piece of birefringent material cut so as to delay one linear polarization component relative to the other by the desired amount (generally either to one half or one quarter of the wavelength of interest). In this case, the phase difference is fixed, and the modulation is accomplished by physically rotating the birefringent plate (and hence the basis of the introduced phase).

In contrast, in this paper we explore a class of polarization modulators in which the basis of phase introduction is held fixed, but the magnitude of the delay is variable. Throughout this paper, we will refer to any device that inserts an adjustable relative delay between two orthogonal linear polarizations as a variable-delay polarization modulator (VPM). There are many examples of devices that implement a variable delay for polarization modulation. For example, Martin[5], and Martin and Puplett[6] describe a version of the Martin–Puplett interferometer (MP) without an input polarizer. VPMs have also been used in several astrophysical polarimetry systems.[7,8] In this work, we explicitly separate the polarization modulation from the polarized detection (analyzer) of the signal. Doing so has two advantages. The first advantage is that the basis of the VPM can be rotated at an arbitrary angle with respect to the orientation of the analyzer. The VPM in a MP is a specific example of this general case in which the relative angle of the VPM is 45° with respect to the analyzer. It should be noted that Martin[5] considers misalignment errors between the beam splitter and the analyzer in a MP. The analytical expression for the polarization in this case is the same for the case of the single VPM placed at an arbitrary angle with respect to the analyzer, although the general physical implementation is different.

The development of the transfer function for a single VPM allows multiple copies of this device to be cascaded at arbitrary relative orientations. We specifically consider the case for two VPMs cascaded in series at appropriate angles so as to fully sample all possible Poincaré states. In this case, we are assuming a narrow enough passband such that the phase delays introduced for the center wavelength approximately apply to the whole band. The VPMs are configured as follows: The VPM that is closest to the polarization-sensitive detector has its beam-splitting grid oriented at an angle of 45° with respect to the axis of the detector (Q axis; see above), and the other VPM has its grid oriented at 22.5° with respect to the detector axes. We show how full modulation of all linear and circular polarization states can be achieved with this device. The use of this architecture in a polarimeter that measures linear polarization can be understood as follows: If we set the device closest to the source (VPM 1) for zero phase delay, and switch the VPM closest to the detector (VPM 2) between delays of 0 and π, then the detector axes, as projected onto the plane of the sky, will switch between Q and $-Q$. With VPM 1 set to a phase delay of π, switching VPM 2 between 0 and π will project the detector axes to $\pm U$. The dual VPMs provide two degrees of freedom, namely the phase delays of the two devices. The angles selected for the two basis sets are those for which the two degrees of freedom correspond to orthogonal coordinates on the Poincaré sphere, thus allowing all polarization states to be accessible to the detector.

There are several qualities that make this architecture a viable candidate technology for future astronomical polarimeters operating in the far infrared through millimeter regions of the spectrum. First, whereas a given birefringent plate can be built to measure either circular or linear polarization, but not both, the VPM allows for implementations that cover the entire Poincaré sphere. Second, since the path difference between orthogonal linear polarization states is variable, these devices are easily retuned for use at multiple wavelengths. Note also that since the VPM requires no transmission through thick dielectric material, frequency-dependent antireflective coatings are not required. Finally, this architecture requires only small linear translations that will eliminate the need for complicated systems of shafts, gears, and bearings that are common in birefringent plate modulators.[9] All of these qualities are beneficial to the future effort to measure the polarized flux of astronomical and cosmological sources from space-borne telescopes.

In Section 2, we derive the Mueller matrix representation of the VPM using the interior part of a MP. Using this result, we calculate the frequency-dependent performance of a VPM in Section 3.

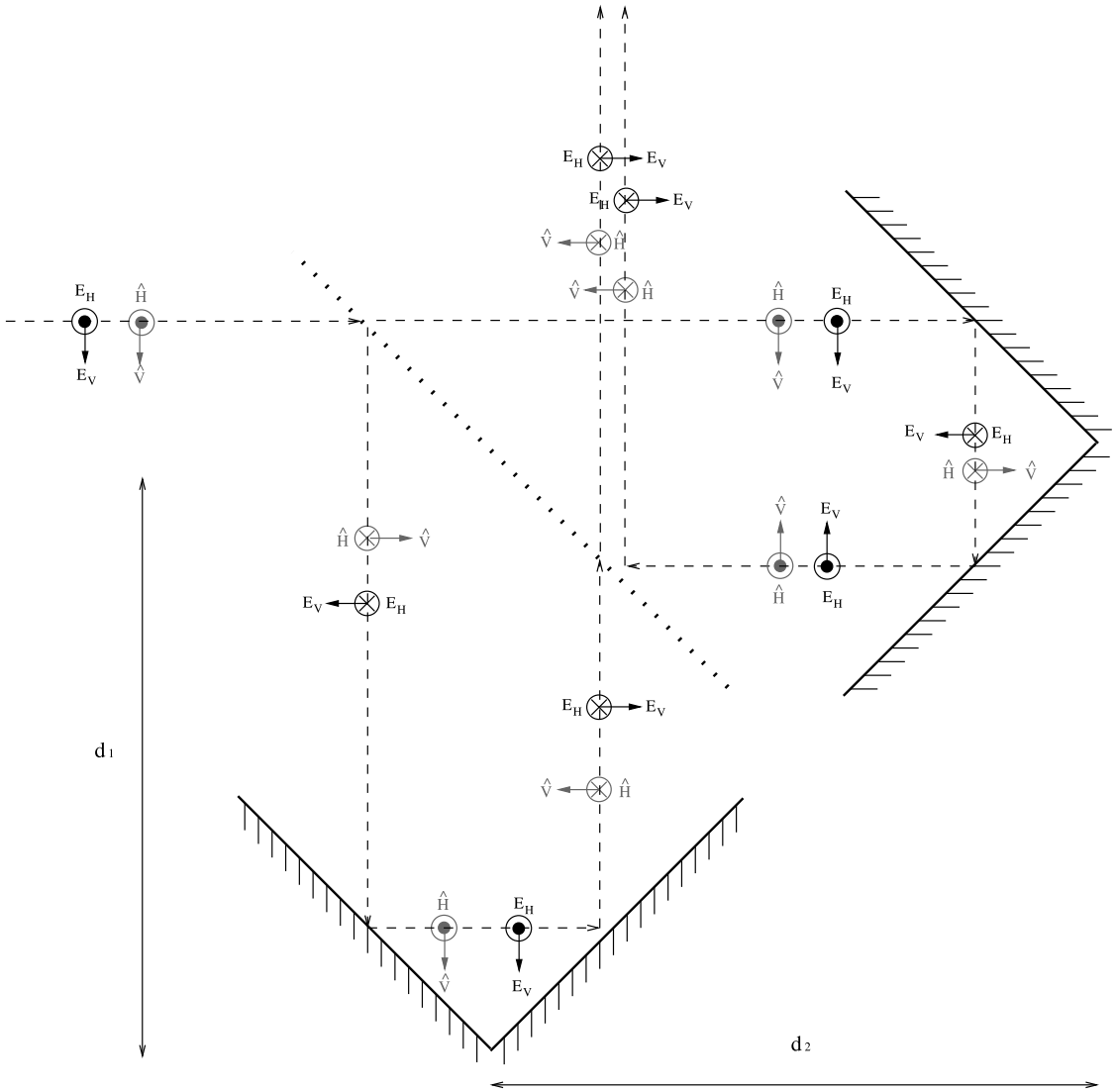

Fig. 1. The propagation of the electric field components and the $(\hat{H}, \hat{V})$ coordinate axes through the VPM part of a Martin–Puplett interferometer at an angle of $\pi/4$ are shown. When $d_1 = d_2$, this device behaves like a mirror. When there is a path difference, it changes the polarization state of the incoming radiation.

Section 4 describes an alternative architecture for the VPM that makes the dual modulator system feasible, Section 5 addresses possible systematics in the application of the VPM, and Section 6 describes laboratory tests to test polarization-modulating properties of a single VPM. We conclude the paper with a brief summary.

2. Single Variable-Delay Polarization Modulator

A Martin–Puplett interferometer consists of a VPM with an analyzer on the output end nominally oriented at an angle of 45° with respect to the beam-splitting grid. For spectrometer applications, one of the ports on the input side is shorted by a grid oriented either parallel or perpendicular to the analyzer. In this section, we use the interior of the MP to generate the Jones and Mueller matrices for a general VPM oriented at an arbitrary angle with respect to the optical system in which it operates. A similar analysis has been done by Martin,[5] but the convenience of standard polarization matrices allows for the subsequent generalization to the case of multiple VPMs in series. For the convenience of the reader, we have included an appendix that briefly describes polarization matrix techniques and elucidates the mathematical conventions that we follow in our analysis.

A diagram of the VPM part of the MP is shown in Fig. 1. Light enters from the left and is split into two orthogonal polarizations by the 45° grid. The two components of polarization are then sent to two rooftop mirrors that rotate the polarization by 90° with respect to the grid wires. The beams recombine at the beam splitter and exit the device at the top.

We will examine this device using Jones matrices, labeling the angle of the device to be the angle of the beam-splitting grid as seen by the incoming radiation. We will first look at the case of a VPM at a rotation of 45° and then generalize to an arbitrary angle using a

similarity transformation. For the simple case, the Jones matrix representing this configuration, $\bar{J}_{\mathrm{VPM}}(\pi/4)$, can be expressed as the sum of the Jones matrices for the radiation in each of the arms of the VPM,

$$\bar{J}_{\mathrm{VPM}}\left(\frac{\pi}{4}\right) = \bar{J}_{\mathrm{VPM}}{}^{(1)}\left(\frac{\pi}{4}\right) + \bar{J}_{\mathrm{VPM}}{}^{(2)}\left(\frac{\pi}{4}\right). \tag{2}$$

In turn, each of these terms can be decomposed into a product of the Jones matrices of the individual elements in each optical path. The Jones matrices for these elements are given in Table 2 in the Appendix.

$$\begin{aligned}\bar{J}_{\mathrm{VPM}}{}^{(1)}\left(\frac{\pi}{4}\right) &= \bar{J}_{\mathrm{WP}}\left(\frac{\pi}{4}\right)\bar{J}_z(d_1)\,\bar{J}_{\mathrm{RT}}(0)\,\bar{J}_z(d_1)\,\bar{J}_{\mathrm{WP}}\left(\frac{\pi}{4}\right)\\ &= \begin{pmatrix}1 & 1\\ -1 & -1\end{pmatrix}\frac{\exp(i4\pi d_1/\lambda)}{2},\end{aligned} \tag{3}$$

$$\begin{aligned}\bar{J}_{\mathrm{VPM}}{}^{(2)}\left(\frac{\pi}{4}\right) &= \bar{J}_{\mathrm{WP}}\left(-\frac{\pi}{4}\right)\bar{J}_z(d_2)\,\bar{J}_{\mathrm{RT}}(0)\,\bar{J}_z(d_2)\,\bar{J}_{\mathrm{WT}}\left(\frac{\pi}{4}\right)\\ &= \begin{pmatrix}1 & -1\\ 1 & -1\end{pmatrix}\frac{\exp(i4\pi d_2/\lambda)}{2}.\end{aligned} \tag{4}$$

Making the definition $\Delta \equiv 4\pi(d_2 - d_1)/\lambda$ and setting $\xi \equiv \Delta/2$, we arrive at the following:

$$\bar{J}_{\mathrm{VPM}}\left(\frac{\pi}{4},\ \xi\right) = \tfrac{1}{2}\mathrm{e}^{i2\pi(d_1+d_2)/\lambda}\begin{pmatrix}\cos\xi & -i\sin\xi\\ i\sin\xi & -\cos\xi\end{pmatrix}. \tag{5}$$

Next, we derive an expression for a VPM placed at an arbitrary angle θ. Recall that the definition of θ we have chosen is the angle of the grid with respect to $\hat{H}$ for the radiation at the input port. To do this, we transform into the coordinate system for which we have already solved the problem, apply the transformation for $\bar{J}_{\mathrm{VPM}}(\pi/4)$, and then transform back. In the case of this architecture, there is a subtlety. Because the number of reflections is odd, the angle of the device as viewed from the outgoing light is the negative of that viewed from the incoming light. This reflection is accounted for in Eq. (6). Setting $\chi = (\theta - \pi/4)$, we note that

$$\bar{J}_{\mathrm{VPM}}(\chi,\ \xi) = \bar{R}^{\dagger}(-\chi)\,\bar{J}_{\mathrm{VPM}}\left(\frac{\pi}{4}\right)\bar{R}(\chi) = \frac{\mathrm{e}^{i2\pi(d_1+d_2)/\lambda}}{2}\begin{pmatrix}\cos\xi + i\sin\xi\sin 2\chi & -i\sin\xi\cos 2\chi\\ i\sin\xi\cos 2\chi & -\cos\xi + i\sin\xi\sin 2\chi\end{pmatrix}, \tag{6}$$

$$\bar{J}_{\mathrm{VPM}}(\theta,\ \xi) = \mathrm{e}^{i2\pi(d_1+d_2)/\lambda}\begin{pmatrix}\cos\xi - i\sin\xi\cos 2\theta & -i\sin\xi\cos 2\theta\\ i\sin\xi\sin 2\theta & -\cos\xi - i\sin\xi\cos 2\theta\end{pmatrix}. \tag{7}$$

In terms of the Stokes parameter basis set, this expression is

$$\begin{aligned}\bar{J}_{\mathrm{VPM}}(\theta,\ \xi) = \mathrm{e}^{i2\pi(d_1+d_2)/\lambda}\{\bar{Q}\cos\xi - i\sin\xi[\bar{I}\cos(2\theta)\\ + i\bar{V}\sin(2\theta)]\}.\end{aligned} \tag{8}$$

Note that within a phase factor (which is irrelevant in a measurement of power) $\bar{J}_{\mathrm{VPM}} = \bar{Q}\bar{J}_{\mathrm{WP}}$. This means that the action of the VPM is equivalent to that of a birefringent plate (having its birefringent axis oriented at an angle θ with a delay $\Delta = 2\xi$) followed by a reflection (represented as the Jones matrix $\bar{Q}$).

The matrix in Eq. (8) is unitary, and its determinant is -1. Thus its Mueller representation is expected to describe symmetries on the Poincaré sphere. By expanding the density matrices in the Pauli matrix basis both before and after performing the similarity transformation corresponding to the optical system, one can generate the Mueller matrix for the system,

$$\bar{M}_{\mathrm{VPM}}(\theta,\ \Delta) = \begin{pmatrix}1 & 0 & 0 & 0\\ 0 & \cos^2 2\theta + \cos\Delta\sin^2 2\theta & -\sin 2\theta\cos 2\theta(1-\cos\Delta) & \sin 2\theta\sin\Delta\\ 0 & \sin 2\theta\cos 2\theta(1-\cos\Delta) & -\sin^2 2\theta - \cos\Delta\cos^2 2\theta & -\cos 2\theta\sin\Delta\\ 0 & \sin 2\theta\sin\Delta & \cos 2\theta\sin\Delta & -\cos\Delta\end{pmatrix}. \tag{9}$$

This matrix can be expressed as a product of symmetry operations on the Poincaré sphere,

$$\begin{aligned}\bar{M}_{\mathrm{VPM}}(\theta,\ \Delta) &= \bar{\Gamma}_{QV}\bar{\Gamma}_{QU}\bar{R}_V(2\theta)\,\bar{R}_Q(\Delta)\,\bar{R}_V(-2\theta)\\ &= \bar{\Gamma}_{QV}\bar{\Gamma}_{QU}\bar{M}_{\mathrm{WP}}(\theta,\Delta).\end{aligned} \tag{10}$$

Here, $\bar{\Gamma}_{QV}$ is a reflection at the Q–V plane, $\bar{\Gamma}_{QU}$ is a reflection at the Q–U plane, $\bar{R}_V$ is a rotation around the V axis, and $\bar{R}_Q$ is a rotation around the Q axis. The matrix $\bar{M}_{\mathrm{WP}}(\theta, \Delta)$ is the Mueller matrix for a wave plate.[10,11]

3. Polarization Modulation

We assume that the detector at the back end of our optical system is sensitive to Stokes Q. This is essentially a statement about the orientation of the analyzer in the polarimetric system. Strictly speaking, a Q sensitive detector requires a differencing of two orthogonal linearly polarized detectors with an orientation that we choose to define the Q axis. However, the following discussion also applies to the class of polarized detector strategies that collect only one linear polarization. Such detectors are technically sensitive to $I \pm Q$, but to lowest order or in ideal modulation, I does not couple to the polarization modulation.

The modulator changes the polarization state of this detector as projected onto the sky. For a single VPM, the polarization state that the detector measured can be calculated from the second column of the Mueller matrix,

$$\begin{aligned} Q_{\mathrm{det}} = {} & Q_{\mathrm{sky}}(\cos^2 2\theta + \cos\Delta \sin^2 2\theta) \\ & + U_{\mathrm{sky}} \sin 2\theta \cos 2\theta(1 - \cos\Delta) \\ & + V_{\mathrm{sky}}(\sin 2\theta \sin\Delta). \end{aligned} \tag{11}$$

For VPM, θ is fixed and Δ is modulated. Using a single VPM, it is not possible to completely modulate Q, U, and V. To see an example of this, consider the case where θ is set to $\pi/4$. In this case,

$$Q_{\mathrm{det}} = Q_{\mathrm{sky}} \cos\Delta + V_{\mathrm{sky}} \sin\Delta. \tag{12}$$

Here, Q and V are modulated, but U is not. This is because at this grid angle, U and $-U$ propagate through the system separately without interfering.

That stated, the advantage of the VPM is that the phase freedom allows a straightforward method for modulating Q and V across large frequency bands. We begin by defining $\Delta \equiv k\delta$, such that $k = 2\pi/\lambda$ and δ is the total path difference between the two orthogonal polarizations. [For the traditional Martin–Puplett beam paths, $\delta = 2(d_2 - d_1)$.] The signal measured by a polarized detector would then be dependent on δ,

$$Q'(k,\ \delta) = Q(k) \cos k\delta + V(k) \sin k\delta. \tag{13}$$

For bolometric detectors, the signal is integrated over the instrument bandpass $\phi(k)$,

$$\begin{aligned} Q'(\delta) &= \int_0^\infty Q'(k',\ \delta)\phi(k')\mathrm{d}k' \\ &= \int_0^\infty [Q(k')\cos k'\delta + V(k')\sin k'\delta]\phi(k')\mathrm{d}k'. \end{aligned} \tag{14}$$

Taking the Fourier transform of both sides yields

$$\tfrac{1}{2}[Q(k) + iV(k)]\phi(\lambda) = \frac{1}{2\pi}\int_{\delta_1}^{\delta_2} Q'(\delta)\, e^{ik\delta}\mathrm{d}\delta. \tag{15}$$

It can be seen that the real part of the Fourier transform of the interferogram is the spectrum of Stokes Q from the source. The imaginary part is the Stokes V spectrum. Note that broadband modulation relies on sampling a large enough range of path length differences.

We note that for the standard implementation of a Martin–Puplett interferometer as a Fourier transform spectrometer, a horizontal or vertical grid is placed at the input port of the device. This sets the input polarization state to be purely Q, thus enabling the internal grid to function as a broadband beam splitter. This is equivalent to shorting one of the input ports. Thus if one makes the reasonable assumption that the polarization of the source is small, then $Q(k) = \frac{1}{2}I(k)$, and Eq. (15) reduces to the unpolarized spectrum of the source. In this case, the device does not measure polarization, but relies on the fact that the input grid is setting the input polarization state to something that is known.

The major disadvantage for this architecture is its insensitivity to Stokes U. For space-borne experiments, U can be recovered by rotation of the spacecraft. For ground-based instruments, sufficient rotation is problematic, and thus an alternative approach may be required.

An alternative to instrument rotation is to place two such devices in series. It is possible to calculate the functional form of the polarization signal on the detectors by simply chaining the two Mueller matrices together. The transfer equation of the optical system is now $\bar{S}_{\mathrm{sky}} = \bar{M}_{\mathrm{VPM}}(\theta_1, \Delta_1)\,\bar{M}(\theta_2, \Delta_2)\,\bar{S}_{\mathrm{det}}$. Note that modulator 2 is closer to the detector than modulator 1. Because our detectors are sensitive to only Q, we solve for the second column of the resulting matrix,

$$\begin{aligned} Q_{\mathrm{det}} = {} & Q_{\mathrm{sky}}\big[(\cos^2 2\theta_1 + \cos\Delta_1 \sin^2 2\theta_1) \\ & \times (\cos^2 2\theta_2 + \cos\Delta_2 \sin^2 2\theta_2) \\ & - \sin 2\theta_1 \cos 2\theta_1 \sin 2\theta_2 \cos 2\theta_2(1 - \cos\Delta_1) \\ & \times (1 - \cos\Delta_2) + \sin 2\theta_1 \sin 2\theta_2 \sin\Delta_1 \sin\Delta_2\big] \\ & + U_{\mathrm{sky}}\big[\sin 2\theta_1 \cos 2\theta_1(1 - \cos\Delta_1) \\ & \times (\cos^2 2\theta_2 + \cos\Delta_2 \sin^2 2\theta_2) \\ & - (\sin^2 2\theta_1 + \cos\Delta_1 \cos^2 2\theta_1)\sin 2\theta_2 \cos 2\theta_2 \\ & \times (1 - \cos\Delta_2) - \cos 2\theta_1 \sin 2\theta_2 \sin\Delta_1 \sin\Delta_2\big] \\ & + V_{\mathrm{sky}}\big[\sin 2\theta_1 \sin\Delta_1(\cos^2 2\theta_2 + \cos\Delta_2 \sin^2 2\theta_2) \\ & + \cos 2\theta_1 \sin 2\theta_2 \cos 2\theta_2 \sin\Delta_1(1 - \cos\Delta_2) \\ & - \sin 2\theta_2 \cos\Delta_1 \sin\Delta_2\big]. \end{aligned} \tag{16}$$

We now consider the specific case where $\theta_1 = \pi/8$ and $\theta_2 = \pi/4$. These angles were carefully chosen to allow full sampling of the Poincaré sphere. Polarized

Table 1. Mapping of Q_{det} onto the Sky for Selected Values of Δ_1 and Δ_2 for Dual Modulators Having $\theta_1 = \pi/8$ and $\theta_2 = \pi/4$

Δ_1	Δ_2	Q_{det}
0	0	Q_{sky}
0	π	$-Q_{sky}$
π	0	U_{sky}
π	π	$-U_{sky}$
0	$\pi/2$	$-V_{sky}$
$\pi/2$	0	$\frac{1}{2}(Q_{sky} + U_{sky}) + \frac{1}{\sqrt{2}}V_{sky}$
$\pi/2$	π	$-\frac{1}{2}(Q_{sky} + U_{sky}) - \frac{1}{\sqrt{2}}V_{sky}$
π	$\pi/2$	V_{sky}
$\pi/2$	$\pi/2$	$\frac{1}{\sqrt{2}}(Q_{sky} + U_{sky})$

sensitivities for selected pairs of phase delay settings for the pair of modulators are shown in Table 1. The simplest method for modulating polarization is to assume a single phase delay over the entire bandwidth. In this case, one sets the modulators to the desired detector polarization sensitivity and makes a measurement. One then repeats this measurement for each state and builds up information about the polarization state of the source.

One of the strengths of this modulator is its ability to modulate quickly between different polarization states. This has the advantage of putting the polarization signal above the $1/f$ knee of the instrument noise spectrum. It may also be possible to extend the bandwidth in a way similar to that of the single modulator above. One could scan these modulators through a range of delays and extract the frequency-dependent Stokes parameters.

4. Other Implementations

The architecture in Fig. 1 is not a unique implementation of a VPM. In fact, there are several arrangements of grids and mirrors that correspond to Jones matrices that differ only by an absolute phase from those that describe the MP as derived above. The simplest of these designs is a system consisting of a polarizing grid placed in front of a mirror. This design is similar in structure to a reflecting wave plate,[12] but in this case, modulation occurs by modulating the grid-mirror spacing rather than by spinning the device. This alternative design for a polarizing interferometer has been previously employed because of its compact features and relative ease of construction.[13] This implementation is useful for a dual modulator system since it requires significantly less space in the optical path than other implementations. The drawbacks are twofold. First, the inability to achieve the zero path length condition causes a slight decrease in effective bandwidth. Second, the two polarizations on the output side of the device are displaced slightly. This effect can be mitigated by using the modulators at close to normal incidence and by placing the modulators as close as possible to a pupil.

5. Systematics

In developing a polarization modulator, one must consider the possibility of instrumental effects introduced by the action of the modulation. In a dielectric half-wave plate, such an effect arises from the absorption properties of a birefringent material. Loss tangents for light polarized along the fast and slow axes are generally different. The result is a modulated signal that appears at twice the rotational frequency of the birefringent plate. For the dual VPM system, there are two important effects to consider. First, for different settings of the translational stage, the edge illumination will change, thereby potentially introducing a spurious polarization signal. This problem can be avoided by restricting the use of such modulators to slow optical systems in which the beam growth through the modulator is minimal. The second concern involves the differential absorption of the grids and the mirrors of the modulator. For the rooftop mirrors, the incident angle of the radiation is the same for different modulator positions. Thus the Fresnel coefficients for each of the two polarizations will remain essentially constant during the modulation process.

6. Experimental Results

A. Setup

To test the polarization modulation of a VPM, we built the MP interferometer configuration illustrated in Fig. 2. The beam exiting the horn attached to port 1 is collimated by an ellipsoidal mirror. It then passes through a polarizing grid that has its wires oriented at 45° angle in projection. Each orthogonal polarization is then launched down a separate arm of the device and reflects off a rooftop mirror that rotates the polarization vector by 90°. The beams recombine at the polarizer and are refocused into the feed connected to port 2. The setup is symmetric, and so the reverse light path is identical. The rooftop mirrors are placed on translational stages such that their relative distances can be adjusted. The frequency-dependent phase that corresponds to this path length difference is the parameter that determines the mapping between polarization states on either end of the device. Note that this system can support ~1 mode in each polarization. Thus Gaussian analysis was used in the design of the optics.[14]

From a microwave circuit perspective, this device is a four-port device with the two ports on either end of the device being defined by the vertically and horizontally polarized electric field modes. We use a Hewlett Packard HP8106D millimeter wave vector network analyzer (VNA) to measure the scattering parameters between these modes. The calibration reference plane is shown (Γ_1 and Γ_2) in Fig. 2. The VNA can be used to measure the 2×2 scattering matrices of pairs of these ports, so to reduce contamination of our results, we place an orthomode transducer[15] (OMT) at the back of each feed horn and terminate the unused polarization with a matched load. For the purposes of these measurements, it is useful to think of the end of

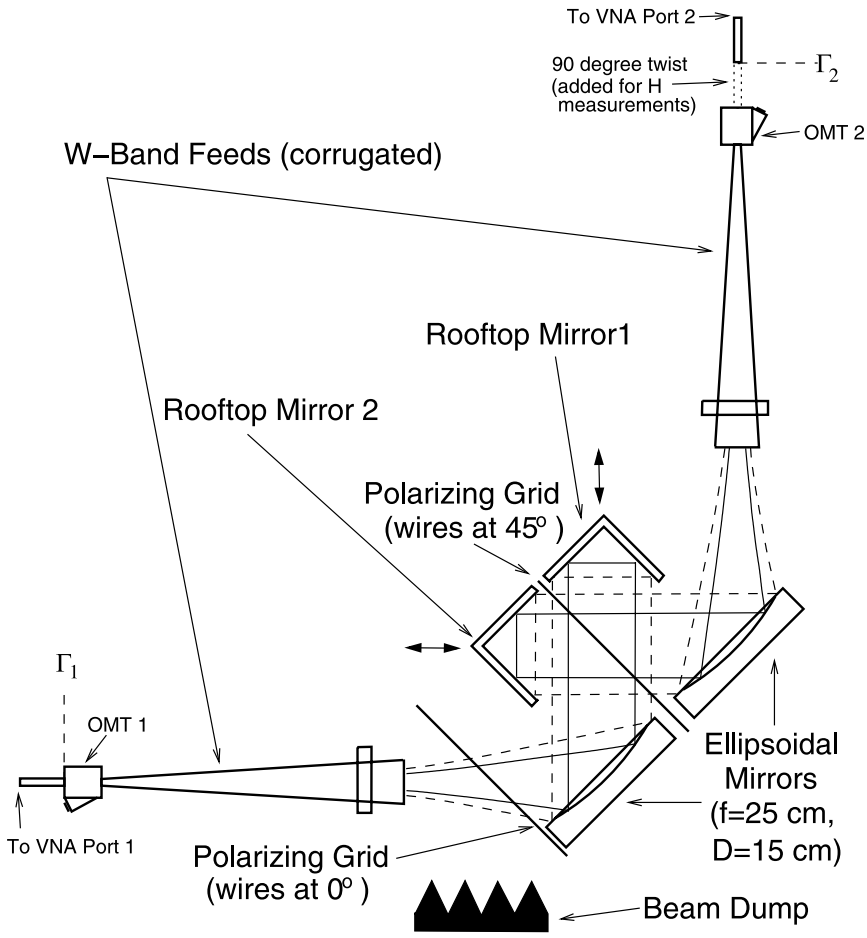

Fig. 2. The Martin–Puplett interferometer is symmetrically fed by a pair of *W*-band feed horns (25–27 dBi) that are collimated by ellipsoidal mirrors (f = 25 cm). Each of the two rooftop mirrors reflect a component of polarizations. The mirrors are mounted on transports that are used to adjust the path lengths of the individual polarizations. The polarizing grid is mounted such that the wires make an angle of 45° with the roof lines in projection. The dashed and dotted lines show the positions of the beam radius (−6.7 dB power level) and –20 dB power level, respectively, of a Gaussian beam propagating through the structure for a 26 dBi feed and a wavelength of 3 mm (100 GHz). We have illustrated the location of the 90° twist on port 2 that converts the sensitivity of port 2 from V to H. The calibration reference plane is also shown (Γ_1 and Γ_2).

the feed horn attached to port 1 of the VNA as the source, and that attached to port 2 as the detector. We set the polarization state of the source to be vertically polarized light (a pure Q state) by orienting the waveguide appropriately. On the detector side, we measure both V and H in successive measurements by, respectively, omitting and adding a 90° twist to the WR-10 waveguide between the OMT and the Γ_2 calibration point. We have measured the loss of the twist to be 0.15 dB. The calibrated difference between the power associated with H and V gives a measurement of Stokes Q at the detector.

The bandwidth of the test setup is approximately 78–115 GHz. At the low end of the band, the band edge is defined by that of the *W*-band feed horns, and at the high end, it is defined by the OMT return loss.

B. Experimental Procedure

We found the zero path length position by first maximizing the signal in the V direction at a point where the S_{21} parameter was flat across the band. We then were able to use the first null condition to do a fine adjustment. V and H are measured for 27 combinations of positions of the two mirrors having path differences corresponding to 24° steps in phase for $\lambda = 3$ mm. Four sample spectra are shown in Fig. 3. We have included in these plots the expected transmission spectra [$H \propto (1 - \cos \Delta)$ and $V \propto (1 - \cos \Delta)$], adopting a global gain of 0.9 dB to account for the expected loss beyond the calibration port. The return loss of the system is about 26 dB and can be seen in the H component of Fig. 3(a). The transmission efficiency of the horns is not constant across the band and tends to roll off at low frequencies.

C. Results

This experimental setup is described mathematically by the expression in Eq. (12). In this case,

$$Q_{\mathrm{det}} = \frac{H(\Delta) - fV(\Delta)}{H(\Delta) + fV(\Delta)} = Q_{\mathrm{source}} \cos \Delta + V_{\mathrm{source}} \sin \Delta, \tag{17}$$

where $\Delta = 4\pi(d_2 - d_1)/\lambda$. Here, $H(\Delta)$ and $V(\Delta)$ are the powers corresponding to S_{21} when the twist is included and excluded, respectively. For each frequency, the relative gain factor, f, is calculated by fitting for the average values of the signals in the H and V configurations and taking the ratio.

For each frequency, it is possible to measure Stokes Q and V. The result of this analysis is shown in Fig. 4. We find that the average Stokes parameters measured over the 78–115 GHz band are $Q = -1.002 \pm 0.003$ and $V = 0.001 \pm 0.013$. There is some nonzero power in Stokes V near the high end

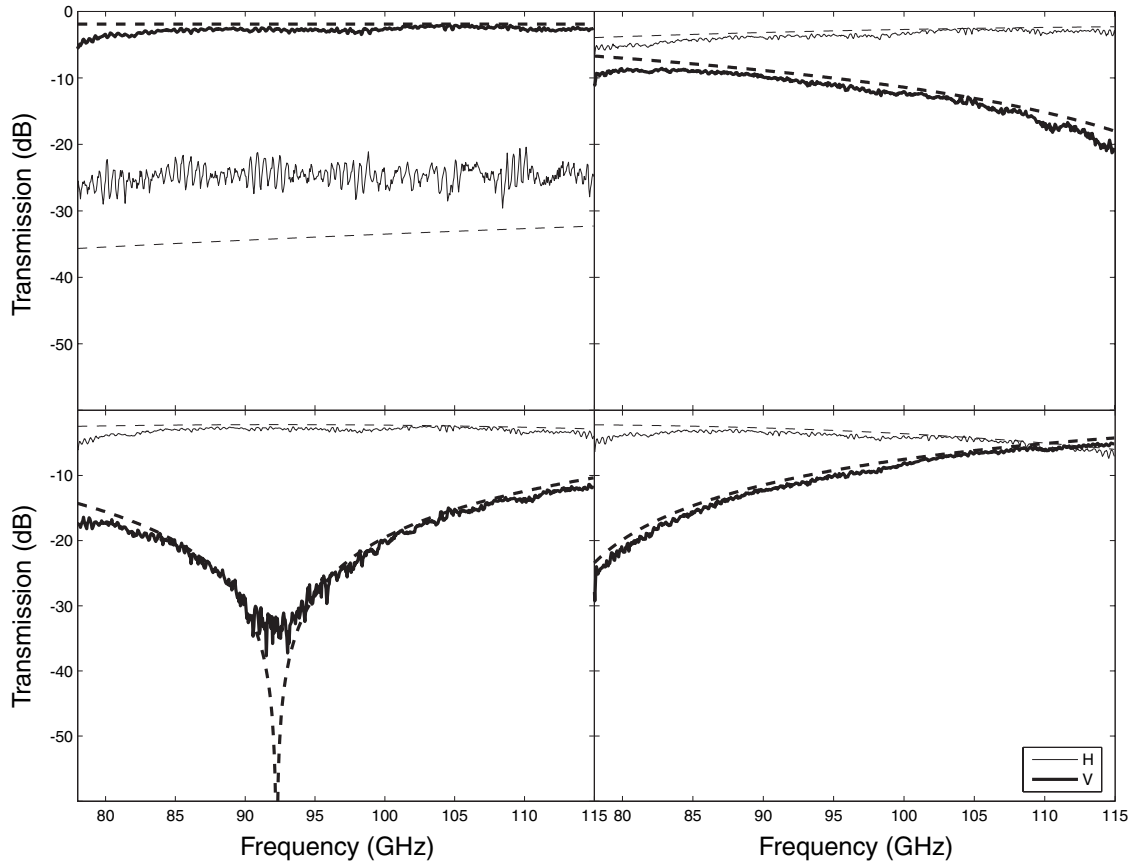

Fig. 3. The transmission spectra are shown for four different values of $d_1 - d_2$: (upper left) -13 μm, (upper right) 587 μm, (lower left) -813 μm, and (lower right) -1013 μm. The thick solid line in each plot is the spectrum of the vertical (V) linear polarization measured at port 2 of the VNA. The thin solid line in each plot is the spectrum of the horizontal (H) linear polarization measured at port 2. The H polarization is measured by adding a 90° twist in the WR-10 waveguide attached to port 2 of the VNA. Theoretical predictions for H and V are plotted as thick and thin dashed lines, respectively.

of the band. It is unclear as to whether this is due to a systematic effect or due to an unknown source polarization.

D. Resonances

In this laboratory setup, proper termination of the unused port at both the entrance and exit apertures is essential, as even small reflections can introduce resonances. These resonances are an indication of the level of uncertainty of phase control of the radiation propagating through the device. This uncertainty directly leads to a frequency-dependent random mixing between the Q and V polarization states and hence a decrease in the precision of the MP as a polarimeter. We have found that this systematic "noise" can be controlled by various levels of termination of the unused polarization. The addition of the OMTs in the signal chain reduced the noise in the transmission from 3 to 1 dB. We also added a horizontal grid at the mouth of the source feedhorn to redirect any residual H component to an eccosorb beam dump. This grid reduced the noise in transmission to 0.25 dB and also reduced the average coupling of Q into V from 4% to under 1%.

On a telescope, this problem is mollified by the fact that the source port is nearly perfectly terminated on the sky. This greatly reduces phase uncertainties in the system as well as the need for excessive polarization filtering.

7. Summary

We have described a technique for polarization modulation in which n phase delays between linear orthogonal polarizations are placed in series with arbitrary relative orientations. We specifically consider the $n = 1$ and $n = 2$ cases, and find that for appropriate relative orientations, it is possible to fully modulate the polarization in the $n = 2$ case. In the far infrared through submillimeter, where bandpasses are typically $\Delta\lambda/\lambda \sim 0.1$, this device can be used in a similar manner to a half-wave plate. Broader bandpasses ($\Delta\lambda/\lambda \sim 0.3$) may be accommodated by using more complex modulation schemes. This architecture enables one to construct a modulator that can be made robust, broadband, and easily tunable to different wavelengths. In addition, it allows for the complete determination of the polarization state of the incoming radiation by the measurement of Stokes Q, U, and V.

It is worth noting one final potential application of

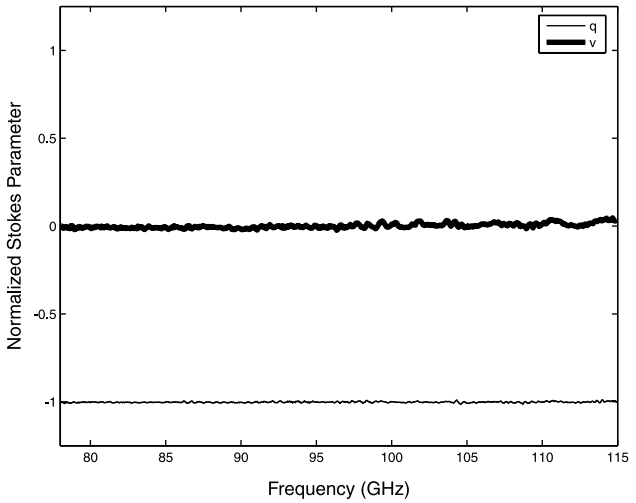

Fig. 4. The normalized Stokes parameters q and v are calculated as a function of frequency by fitting to the 27 mirror positions. The mean values of q and v across the 78–115 GHz band are -1.002 ± 0.003 and 0.001 ± 0.013, respectively.

VPMs. The ability of these devices to work at room temperature may make them useful as calibrators. An input polarized signal can be transformed quite easily to test the polarization response of a precision polarization sensor. It can transform an initially linearly polarized state into an elliptical polarization state.

Appendix A: Polarization Matrix Methods

In this appendix, we review the properties of Jones, density, and Mueller matrices and their relationships.

A. Jones Matrices

Jones matrices[16] are a convenient way to analyze radiation as it propagates through an optical system in architectures in which it is important to keep track of phase. For the ideal case, we assume that all ports are matched and so no cavities are formed. This formulation is applicable for coherent radiation; however, it can be extended using the closely related formalism of density matrices to treat the problem of partially polarized light.[17]

Jones matrices are 2×2 matrices that contain information about how the orthogonal electric field components transform in an optical system. The input Jones vector is defined as follows:

$$|E\rangle = \begin{pmatrix} E_x \\ E_y \end{pmatrix} \equiv \begin{pmatrix} E_H \\ E_V \end{pmatrix}. \tag{A1}$$

The output vector from an optical system can then be represented by $|E_f\rangle = \bar{J}|E_i\rangle$ where $\bar{J}$ is the vector transformation introduced by the optical system. The power measured at a detector at the back end of such a system is given by

$$\langle E_f|\bar{J}_{\mathrm{det}}|E_f\rangle = \langle E_i|\bar{J}^{\dagger}\,\bar{J}_{\mathrm{det}}\,\bar{J}|E_i\rangle. \tag{A2}$$

The matrix $\bar{J}_{\mathrm{det}}$ is dependent on the properties of the detector used to make the measurement.

In the Jones matrix representation, Stokes parameters are represented by the Pauli matrices and the identity matrix.

$$\bar{I} \equiv \bar{\sigma}_0 = \begin{pmatrix} 1 & 0 \\ 0 & 1 \end{pmatrix}, \quad \bar{Q} \equiv \bar{\sigma}_1 = \begin{pmatrix} 1 & 0 \\ 0 & -1 \end{pmatrix},$$

$$\bar{U} \equiv \bar{\sigma}_2 = \begin{pmatrix} 0 & 1 \\ 1 & 0 \end{pmatrix}, \quad \bar{V} \equiv \bar{\sigma}_3 = \begin{pmatrix} 0 & -i \\ i & 0 \end{pmatrix}. \tag{A3}$$

We will use the convention that a bar over the Stokes symbol indicates its Jones matrix representation. An unbarred Stokes parameter represents measurable power (e.g., $Q = \langle E|\bar{Q}|E\rangle$). Note that the measured power in each of the Stokes parameters is

$$I = \langle E|\bar{I}|E\rangle = E_H{}^2 + E_V{}^2, \tag{A4}$$

$$Q = \langle E|\bar{Q}|E\rangle = E_H{}^2 - E_V{}^2, \tag{A5}$$

$$U = \langle E|\bar{U}|E\rangle = 2\,\Re(E_H{}^* E_V), \tag{A6}$$

$$V = \langle E|\bar{V}|E\rangle = 2\,\Im(E_H{}^* E_V). \tag{A7}$$

These equations connect the Jones matrix formulations of the Stokes parameters to their familiar definitions.[3,18] These four Stokes matrices have the following multiplicative properties. Defining $(\bar{\sigma}_0, \bar{\sigma}_1, \bar{\sigma}_2, \bar{\sigma}_3) \equiv (\bar{I}, \bar{Q}, \bar{U}, \bar{V})$, $\bar{\sigma}_0\bar{\sigma}_\alpha = \bar{\sigma}_\alpha\bar{\sigma}_0 = \bar{\sigma}_\alpha$ for $\alpha \in (0, 1, 2, 3)$ and $\bar{\sigma}_j\bar{\sigma}_k = \sum_l \epsilon_{jkl} i\bar{\sigma}_l + \delta_{jk}\bar{\sigma}_0$ for $j, k, l \in (1, 2, 3)$. These four matrices form a convenient basis for expressing Jones matrices. Table 2 shows both the explicit Jones matrices and the Stokes expansion for selected optical transformations. The mirror transformation, which can be expressed simply as $\bar{Q}$, sets the convention for how the $(\hat{H}, \hat{V})$ coordinate system is propagated through the optical system. Note that for some structures, the Stokes expansion provides a convenient way to express optical elements. Successive transformations can be calculated either by matrix algebra or by the Pauli algebra defined above.

B. Density Matrices

In the general case of partially polarized light, polarization arises because of time-averaged (statistical) correlations between the electric field components. The density matrix is a complex 2×2 matrix that fully characterizes the polarization state of the light. It is given by

$$\bar{D} = \begin{pmatrix} \langle E_x{}^* E_x\rangle & \langle E_x{}^* E_y\rangle \\ \langle E_y{}^* E_x\rangle & \langle E_y{}^* E_y\rangle \end{pmatrix}. \tag{A8}$$

Here, the brackets indicate a time average. If the density matrix is expressed as a linear combination of

Table 2. Summary of Jones Matrix Representations for Selected Optical Elements[a]

Description	Symbol	Matrix Representation	Stokes Expansion
Linear distance	$\bar{J}_z(d)$	$\begin{pmatrix} \exp(i2\pi d/\lambda) & 0 \\ 0 & \exp(i2\pi d/\lambda) \end{pmatrix}$	$\bar{I}\exp(i2\pi d/\lambda)$
Mirror	$\bar{J}_M$	$\begin{pmatrix} 1 & 0 \\ 0 & -1 \end{pmatrix}$	$\bar{Q}$
Wire grid (ref.)	$\bar{J}_{WP}(\theta)$	$\begin{pmatrix} \cos^2\theta & \sin\theta\cos\theta \\ -\sin\theta\cos\theta & -\sin^2\theta \end{pmatrix}$	$\frac{1}{2}(\bar{Q} + \bar{I}\cos 2\theta + i\bar{V}\sin 2\theta)$
Wire grid (trans.)	$\bar{J}_{WT}(\theta)$	$\begin{pmatrix} \sin^2\theta & -\sin\theta\cos\theta \\ -\sin\theta\cos\theta & -\cos^2\theta \end{pmatrix}$	$\frac{1}{2}(\bar{I} - \bar{Q}\cos 2\theta - \bar{U}\sin 2\theta)$
Coord. rotation	$\bar{R}(\theta)$	$\begin{pmatrix} \cos\theta & \sin\theta \\ -\sin\theta & \cos\theta \end{pmatrix}$	$\bar{I}\cos\theta + i\bar{V}\sin\theta$
Rooftop mirror	$\bar{J}_{RT}$	$\begin{pmatrix} \cos 2\theta & \sin 2\theta \\ \sin 2\theta & \cos 2\theta \end{pmatrix}$	$\bar{I}\cos 2\theta + i\bar{V}\sin 2\theta$
Birefringent plate	$\bar{J}_{WP}(\theta, \xi)$	$\begin{pmatrix} \cos\xi - i\sin\xi\cos 2\theta & -i\sin\xi\sin 2\theta \\ -i\sin\xi\sin 2\theta & \cos\xi + i\sin\xi\cos 2\theta \end{pmatrix}$	$\bar{J}\cos\xi - i\sin\xi(\bar{Q}\cos 2\theta + \bar{U}\sin 2\theta)$

[a]The Jones matrix representations and the Pauli algebra representations are given (Ref. 19). For the linear distance transformation, d represents the distance traveled. For the mirror, a rotation of the mirror has no effect, and thus $\bar{Q}$ is a general representation for this element. For the wire grid, θ is the angle of the grid wires with respect to the $\hat{H}$ axis. For the rooftop mirror, θ is the angle between the roof line and the $\hat{H}$ axis. For the birefringent plate, θ is the angle between the fast axis of birefringence and the $\hat{H}$ axis, and ξ is half of the phase delay introduced between the orthogonal polarizations.

the Pauli matrices, $\bar{D} = I\bar{\sigma}_0 + Q\bar{\sigma}_1 + U\bar{\sigma}_2 + V\bar{\sigma}_3$, the coefficients are the Stokes parameters.

The transformation of the polarization state by an optical system is given by a similarity transformation, $\bar{D}' = \bar{J}^\dagger\bar{D}\bar{J}$. Here, $\bar{J}$ is the Jones matrix describing the optical system. For the purposes of this paper, we are interested in how the polarization state of the detectors map onto the sky, and so $\bar{D}_{sky} = \bar{J}^\dagger\bar{D}_{det}\bar{J}$. Note the similarity in the transformation of the density matrix and the expression for total power in the Jones matrix formalism [Eq. (A2)].

C. Mueller Matrices

Until now, no limitations have been placed on $\bar{J}$, the matrix describing an optical system under consideration. If the magnitude of the determinant of $\bar{J}$ is unity, then there is a homomorphism between the group of 2×2 matrices having $|\det(\bar{J})| = 1$ and the Poincaré or inhomogenous Lorentz group. In this case, the quantity $I^2 - Q^2 - U^2 - V^2$ is preserved under these transformations. In analogy to special relativity,[20] the inhomogeneous Lorentz group can be represented by a group of 4×4 real matrices acting on a Stokes vector, $\bar{S} = (I, Q, U, V)$. These matrices are known as Mueller matrices. For our purposes, we consider the Mueller matrix that maps the Stokes parameters at the detector to the sky: $\bar{S}_{sky} = \bar{M}\bar{S}_{det}$.

For polarization modulation, we are particularly interested in the case for which the Jones matrices describing our optical system are unitary. In this case, Stokes I decouples from the other Stokes parameters and the quantity $P^2 = Q^2 + U^2 + V^2$ is preserved. This subgroup can be represented by 3×3 orthogonal submatrices that represent symmetries on the surface of a sphere in a space having Stokes Q, U, and V as axes. This sphere is called the Poincaré sphere.

As an aside we note that if we restrict the group of density matrices to those with positive determinants, the system is described by SU(2), and thus there is a homomorphism between this group and SO(3), the group of rotations on the Poincaré sphere. These are the groups that are important to a wave plate; however, the physical reflection involved in the VPM architecture introduces a negative determinant, resulting in combinations of rotations and reflections on the Poincaré sphere.

The authors thank Don Jennings for his useful discussions on polarimetry; Dale Fixsen for his help with the manufacturing of the collimators; Terry Doiron for supplying the grids; and Gary Hinshaw, Dominic Benford, and Al Kogut for their support of this work. This work was funded by a NASA GSFC DDF award and by NASA ROSS APRA grant APRA04-007-0150.

References

1. W. S. Holland, W. Duncan, B. D. Kelly, K. D. Irwin, A. J. Walton, P. A. R. Ade, and E. I. Robson, "SCUBA-2: a new generation submillimeter imager for the James Clerk Maxwell Telescope," in *Millimeter and Submillimeter Detectors for Astronomy,* T. G. Phillips and J. Zmuidzinas, eds., Proc. SPIE **4855,** 1–18 (2003).
2. D. A. Harper, A. E. Bartels, S. C. Casey, D. T. Chuss, J. L. Dotson, R. Evans, S. Heimsath, R. A. Hirsch, S. Knudsen, R. F. Loewenstein, S. H. Moseley, M. Newcomb, R. J. Pernic, T. S. Rennick, E. Sandberg, D. B. Sandford, M. L. Savage, R. F. Silverberg, R. Spotz, G. M. Voellmer, P. W. Waltz, S. Wang, and C. Wirth, "Development of the HAWC far-infrared camera

for SOFIA," in *UV and Gamma-Ray Space Telescope Systems,* G. Hasinger and M. J. L. Turner, eds., Proc. SPIE **5492,** 1064–1073 (2004).
3. J. Tinbergen, *Astronomical Polarimetry* (Cambridge, 1996).
4. R. H. Hildebrand, J. A. Davidson, J. L. Dotson, C. D. Dowell, G. Novak, and J. E. Vaillancourt, "A primer on far-infrared polarimetry," Publ. Astron. Soc. Pac. **112,** 1215–1235 (2000).
5. D. H. Martin, in *Infrared and Millimeter Waves,* J. Button, ed. (Academic Press, 1974), Vol. 6.
6. D. Martin and E. Puplett, "Polarised interferometric spectrometry for the millimetre and submillimetre spectrum," Infrared Phys. **10,** 105–109 (1970).
7. E. Battistelli, M. DePetris, L. Lamagna, R. Maoli, F. Melchiorri, E. Palladino, and G. Savini, "Far infrared polarimeter with very low instrumental polarization," arXiv.org e-Print archive, version 1, astro-ph/0209180, http://arxiv.org/astro-ph/astro-ph/0209180.
8. P. Lubin (personal communication).
9. B. R. Johnson, M. E. Abroe, P. Ade, J. Bock, J. Borrill, J. S. Collins, P. Ferreira, S. Hanany, A. H. Jaffe, T. Jones, A. T. Lee, L. Levinson, T. Matsumura, B. Rabii, T. Renbarger, P. L. Richards, G. F. Smoot, R. Stompor, H. T. Tran, and C. D. Winant, "MAXIPOL: a balloon-borne experiment for measuring the polarization anisotropy of the cosmic microwave background radiation," New Astron. Rev. **47,** 1067–1075 (2003).
10. K. Serkowski, in *Methods of Experimental Physics,* N. Carleton, ed. (Academic, 1974), Vol. 12.
11. G. Novak, D. Gonatas, R. Hildebrand, and S. Platt, "A 100-μm polarimeter for the Kuiper Airborne Observatory," Publ. Astron. Soc. Pac. **101,** 215–224 (1989).
12. G. Siringo, E. Kreysa, L. A. Reichertz, and K. M. Menten, "A new polarimeter for (sub)millimeter bolometer arrays," Astron. Astrophys. **422,** 751–760 (2004).
13. T. Manabe, J. Inatani, A. Murk, R. J. Wylde, M. Seta, and D. H. Martin, "A new configuration of polarization-rotating dual-beam interferometer for space use," IEEE Trans. Microwave Theory Tech. **51,** 1696–1704 (2003).
14. P. F. Goldsmith, *Quasioptical Systems* (IEEE Press, 1998).
15. E. Wollack and W. Grammer, "Symmetric waveguide orthomode junctions," in *Proceedings of the 14th International Symposium on Space TeraHertz Technology,* E. Walker and J. Payne, eds. (2003), pp. 169–176.
16. R. Jones, "New calculus for the treatment of optical systems," J. Opt. Soc. Am. **31,** 488–493 (1941).
17. C. Brosseau, *Fundamentals of Polarized Light* (Wiley, 1998).
18. J. Jackson, *Classical Electrodynamics* (Wiley, 1967).
19. D. E. Budil, Z. Ding, G. R. Smith, and K. A. Earle, "Jones matrix formalism for quasioptical EPR," J. Magn. Reson. **144,** 20–34 (2000).
20. S. Sternberg, *Group Theory and Physics* (Cambridge, 1994).